International Journal of Heat and Technology
Vol. 44, No. 3, June, 2026, pp. 1133-1148
Journal homepage: http://iieta.org/journals/ijht

Coupled Heat and Mass Transfer and Thermodynamic Response Characteristics of Surrounding Rock in Underground Tunnels

Wenkai Jiang, Yigang You*

Business School, Guangxi University of Finance and Economics, Nanning 530007, China

Corresponding Author Email: YouYG@gxufe.edu.cn

https://doi.org/10.18280/ijht.440321

Received: 10 January 2026
Revised: 8 May 2026
Accepted: 23 May 2026
Available online: 30 June 2026

Keywords:
underground tunnels, porous media, coupled heat and mass transfer, thermodynamic response, surrounding rock stability, multi-field coupling

ABSTRACT

In high-geothermal environments, significant heat and mass interaction occurs within the surrounding rock of underground tunnels. The resulting multi-field coupled evolution and associated thermodynamic instability represent a core challenge to the long-term safety of deep tunnel engineering. Current research hinders the accurate characterization of non-steady-state heat and mass transfer and the underlying mechanisms of thermodynamic response. Taking a deep high-geothermal tunnel as the research context, and grounded in the fundamental theory of coupled heat and mass transfer in porous media, a refined numerical model was developed to represent the dynamic interactive effects within the surrounding rock. A systematic investigation was then conducted on the spatiotemporal evolution of heat and mass behavior and the associated thermodynamic response characteristics. By analyzing the synergistic feedback mechanism between thermal conduction and moisture migration, the dynamic evolution of temperature, humidity, and stress fields was examined under varying burial depths, ambient temperatures, and petrophysical properties. The complete mechanism of pore structure evolution, mechanical property degradation, and overall instability under coupled heat and mass action was thereby elucidated. The results indicate that tunnel excavation disturbs the inherent heat and mass equilibrium of the surrounding rock, significantly accelerating internal transfer rates and generating a concentrated zone of coupled response in the shallow layer. The temperature-gradient-driven directional moisture migration reshapes the pore structure distribution, induces continuous redistribution of thermal stress, and ultimately leads to cracking, deformation, and a decay in load-bearing capacity. The bidirectional dynamic heat and mass coupling is identified as the primary trigger for thermodynamic damage and instability in high-geothermal tunnel surrounding rock. Furthermore, the intensity of the thermodynamic response exhibits a significant power-law growth with increasing ambient temperature and burial depth. This study clarifies the core mechanisms governing coupled heat and mass transfer in high-geothermal tunnel rock masses, enriches the theoretical framework of multi-field coupling thermodynamics for deep tunnels, and provides a theoretical basis and technical reference for stability control, support structure optimization, and long-term operational safety in high-temperature tunnel engineering.

1. INTRODUCTION

The development and construction of deep underground engineering projects have been progressively extended into the complex stratigraphic formations and deep geological environments of western China. Consequently, the issue of high-geothermal hazards in deep-buried tunnels has become increasingly prominent, representing a core challenge to the safe construction and long-term serviceability of deep geotechnical engineering [1, 2]. The in-situ high-geothermal environment of deep strata, combined with the disturbances induced by tunnel excavation unloading and groundwater seepage, gives rise to intense heat transfer and moisture migration behavior within the surrounding rock, thereby triggering compound engineering thermal hazards [3, 4]. In numerous high-altitude deep-buried tunnel projects across China, conditions involving the coexistence of extremely high-temperature surrounding rock and high-temperature groundwater have been observed. This severe thermal-humid environment not only significantly compromises the operational safety and work efficiency of construction personnel, but also persistently erodes the tunnel lining structure, accelerating its cracking, aging, and failure. Simultaneously, it induces internal stress redistribution and fracture propagation within the surrounding rock, substantially degrading its overall stability [5, 6]. The heat and mass transfer process in tunnel surrounding rock is a quintessential nonlinear, multi-physical field coupling evolution process. Thermal driving forces govern internal heat conduction and fluid convection, modifying the fundamental thermal properties of the rock mass and the occurrence state of groundwater. Seepage flow transports heat across spatial domains, altering the effective stress state of the surrounding rock through variations in pore pressure. The dynamic adjustment of the stress field further reshapes the fracture structure and permeability characteristics of the rock mass, thereby exerting a feedback control on the transport pathways for both heat and fluid [7, 8]. The coupled effects arising from this dynamic multi-physical field interaction directly govern the damage evolution and instability processes in high-geothermal tunnel surrounding rock. A systematic elucidation of the coupled heat and mass transfer mechanisms and the associated thermodynamic response characteristics in deep-buried tunnel surrounding rock is therefore essential. Such an understanding serves not only to advance the fundamental theory of multi-field coupling in deep rock masses, but also to provide a reliable theoretical foundation and engineering basis for the prevention and control of thermal hazards, ventilation optimization, and support system design in high-geothermal tunnels [9, 10].

Extensive theoretical, experimental, and numerical investigations have been conducted on the coupled thermal-hydraulic-mechanical behavior of fractured rock masses, progressively establishing a multi-field coupling analysis framework suitable for underground rock engineering [11, 12]. In early studies, the local thermal equilibrium assumption was commonly adopted, wherein the fractured rock mass was treated as an equivalent homogeneous continuum, with the temperature of the rock skeleton and the internal fluid assumed to remain consistent. This approach effectively simplified the solution of multi-field coupling problems and proved applicable to tunnel engineering analyses under conventional temperature conditions [13, 14]. To accommodate the complex conditions inherent in deep high-geothermal engineering, the local thermal non-equilibrium theory has been progressively applied to heat transfer studies in rock masses. By distinguishing the temperature difference between the rock skeleton and the fracture fluid, this theory enables an accurate representation of the heat exchange process between the solid and liquid phases under high-temperature conditions, effectively remedying the limitations of the traditional thermal equilibrium theory [15, 16]. Through sustained development, substantial progress has been achieved in the theoretical modeling, numerical simulation, and engineering application of multi-field coupling in rock masses [17]. Nevertheless, significant systematic deficiencies remain within the existing research framework. Most thermal non-equilibrium theoretical models are restricted to the analysis of a single heat transfer process, without incorporating the mechanical response mechanism into a unified coupling framework. Consequently, these models are incapable of elucidating the stress evolution and surrounding rock damage mechanisms induced by solid-liquid temperature differentials, and a complete mathematical characterization system for fully coupled thermal-hydraulic-mechanical processes remains absent. Furthermore, prevailing numerical simulation studies commonly prescribe core thermal properties, such as thermal conductivity and specific heat capacity of the rock mass, as fixed constants [18], while neglecting the nonlinear evolution characteristics of these parameters under coupled thermal and stress effects. However, laboratory experiments have confirmed that variations in temperature and pressure conditions significantly modify the thermophysical properties of rock masses. The adoption of constant parameter values can introduce considerable deviations in the computed thermodynamic responses, severely compromising the accuracy of numerical analyses [19, 20]. In addition, current thermal hazard assessment approaches for high-geothermal tunnels remain relatively simplistic, relying solely on dry-bulb temperature for safety evaluations. This practice neglects the synergistic effects of multiple factors—including humidity, airflow velocity, and thermal radiation—under high-temperature and high-humidity conditions. As a result, an accurate characterization of the true thermodynamic state of the surrounding rock and the on-site thermal hazard level cannot be achieved, impeding the implementation of refined hazard classification and scientifically based prevention strategies [21, 22].

To address the deficiencies in theoretical modeling, parameter characterization, and engineering evaluation prevalent in existing studies, a systematic and integrated research framework is established. An in-depth investigation is conducted on the coupled heat and mass transfer and thermodynamic response characteristics of surrounding rock in high-geothermal tunnels, yielding multiple core innovative contributions. A dual-medium fully coupled thermal-hydraulic-mechanical numerical model is developed based on the local thermal non-equilibrium theory, enabling the synergistic solution of multi-physical field variables and elucidating the microscopic thermodynamic mechanisms of heat and mass transfer in surrounding rock under non-equilibrium conditions. The coupling effects of temperature variation and stress have been embedded into the model, establishing a dynamic bidirectional feedback mechanism between thermophysical properties of the rock mass and the multi-physical fields, thereby overcoming the limitations of conventional constant-property modeling. Furthermore, a comprehensive classification and evaluation system for tunnel thermal-humid environments has been established by integrating multi-dimensional thermodynamic evaluation indicators, facilitating a scientific and refined assessment of thermal hazards in high-geothermal tunnels.

This study is organized into six chapters, with the overall research logic progressing in a hierarchical and coherent manner. Chapter 1 provides a review of the engineering background and the current state of domestic and international research, identifying the deficiencies in existing studies, and delineating the core research content and innovative contributions of this work. In Chapter 2, key thermophysical parameters of the surrounding rock are obtained through laboratory testing, with the evolution of these parameters as functions of temperature and stress systematically revealed and corresponding constitutive relationships formulated. Chapter 3 presents the derivation of the multi-field coupled governing equations and the construction of a complete theoretical model for coupled heat and mass thermodynamics. Chapter 4 establishes the numerical solution methodology, with model reliability validated through multiple sets of comparative tests and engineering monitoring data. In Chapter 5, parametric analyses are conducted under various working conditions using the validated model, identifying the dominant controlling factors and evolution patterns of the thermodynamic response of the surrounding rock. Optimization recommendations for engineering prevention and control are proposed in conjunction with the classification and evaluation system. Chapter 6 synthesizes the core conclusions of the study, summarizes the application value of the research findings, and outlines directions for future in-depth investigations.

2. LABORATORY DETERMINATION OF THERMOPHYSICAL PARAMETERS OF SURROUNDING ROCK

2.1 Multi-field coupled test platform and specimen preparation

The rock specimens used in this study were collected from intact granite formations encountered in a deep-buried, high-geothermal tunnel located in southwestern China, with the maximum in-situ measured temperatures of the surrounding rock and groundwater reaching 88.8 ℃ and 63.4 ℃, respectively, which realistically reproduces the occurrence environment and thermal hazard conditions of deep high-temperature strata. All specimens were machined into standard cylindrical shapes in strict accordance with the International Society for Rock Mechanics standards, with precise control over specimen dimensions and end-surface flatness, thereby eliminating geometric errors from the specimen preparation stage that could interfere with the test results. The experiments were conducted using a self-modified thermal-hydraulic-mechanical coupled triaxial testing system. This equipment overcomes the limitations of conventional single-dimension testing in geotechnical thermal-mechanical experiments by integrating a transient plane source thermal property testing module and a steady-state seepage heat transfer combined testing module, enabling simultaneous and continuous measurement of thermophysical properties and seepage characteristics of the same specimen under multi-field coupled conditions. A dual-helix sensor structure was employed in the experiments to serve both as a heat source supply and for time-series temperature data acquisition, with a fixed heating power and data acquisition duration established. An ultra-high goodness-of-fit was adopted as the criterion for validating effective experimental data. Meanwhile, contact thermal resistance was eliminated through the filling of a high-thermal-conductivity medium at the contact interfaces, and precise and constant experimental conditions were maintained using a high-precision temperature control and servo pressure system. To accurately isolate the independent mechanisms of temperature, confining pressure, and artificial fracture structures on the heat and mass transfer characteristics of the rock mass, three differentiated specimen groups were established, corresponding to test conditions for temperature evolution, stress evolution, and fracture seepage heat transfer, respectively. Multiple parallel specimens were configured for each group and repeat tests were conducted, with stepwise constant-temperature and constant-pressure experimental procedures employed to eliminate cross-interference among multiple fields, thereby ensuring the stability and reliability of the experimental data. Figure 1 presents a schematic diagram of the thermal-hydraulic-mechanical multi-field coupled triaxial testing system and specimen preparation.

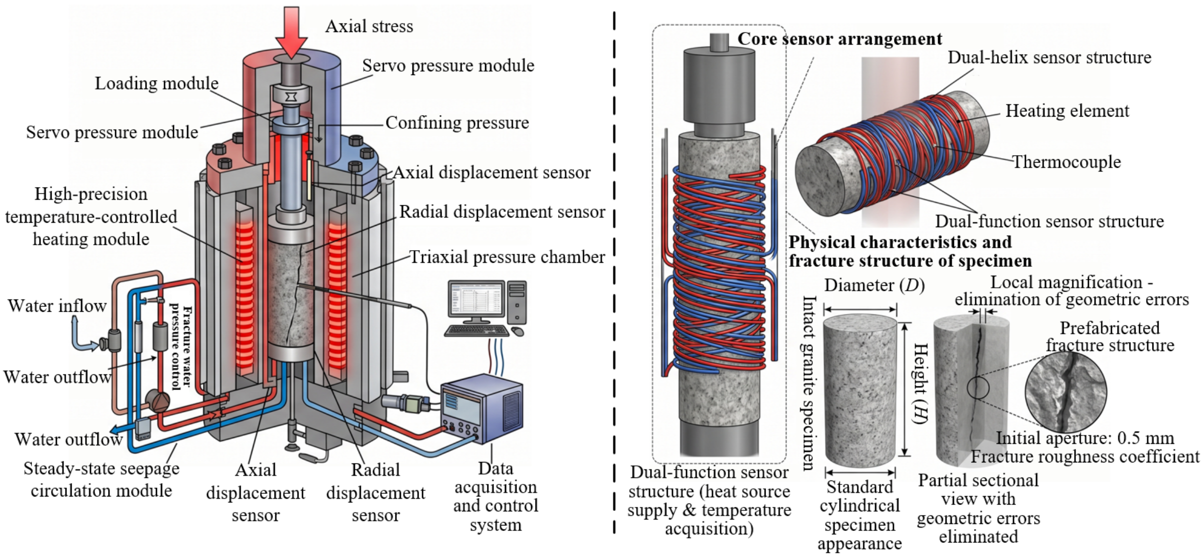

Figure 1. Schematic diagram of the thermal-hydraulic-mechanical multi-field coupled triaxial testing system and specimen preparation

2.2 Evolution of thermophysical parameters with temperature and its constitutive characterization

Through thermal-mechanical tests conducted on rock specimens under gradient temperature conditions ranging from 25 ℃to 100 ℃, the nonlinear evolution of key thermophysical parameters of granite surrounding rock under high-geothermal environments was systematically revealed. The test results indicate that an increase in formation temperature significantly alters the fundamental heat transfer performance of the rock mass. The thermal conductivity of the rock mass was found to continuously decrease with rising temperature, with values declining from 3.42 W/(m·K) to 2.56 W/(m·K), representing a total attenuation of 25.1%. Meanwhile, the specific heat capacity of the rock mass exhibited a steady increase with temperature elevation, with an increase of 23.0%. The thermal diffusivity, being jointly determined by thermal conductivity and volumetric specific heat capacity, was subject to the superimposed effects of their opposing evolution trends, resulting in an overall reduction of 39.2%, which constitutes the most temperature-sensitive indicator among the three core thermophysical parameters. At the microscopic mechanism level, temperature elevation intensifies the lattice vibrations of minerals within the rock mass, shortens the mean free path of phonon heat transfer, and weakens the solid-phase heat conduction capacity, ultimately manifesting as a reduction in thermal conductivity. Concurrently, the degrees of freedom of lattice vibrations continuously increase with rising temperature, necessitating more heat to elevate the temperature per unit mass of the rock, which macroscopically presents as a positive growth characteristic of specific heat capacity. To achieve accurate quantitative characterization of thermophysical parameters and satisfy the requirements for dynamic parameter iteration in subsequent multi-field coupled numerical models, a second-order polynomial temperature-corrected constitutive model was established, with room temperature (25 ℃) adopted as the reference temperature. This model quantitatively describes the nonlinear evolution characteristics of thermophysical parameters with temperature, with the specific expressions given as follows:

$$f_\lambda(T)=1+a_1(T-T_0)+a_2(T-T_0)^2 \tag{1}$$

$$f_c(T)=1+b_1(T-T_0)+b_2(T-T_0)^2 \tag{2}$$

where, $f_\lambda(T)$ and $f_c(T)$ denote the temperature correction coefficients for thermal conductivity and specific heat capacity, respectively; T is the real-time test temperature; T_0 is the reference temperature; a_1 and a_2 are the temperature fitting coefficients for thermal conductivity; and b_1 and b_2 are the temperature fitting coefficients for specific heat capacity. Least-squares fitting calculations were performed based on the measured experimental data, yielding the quantitative values of each fitting coefficient. The coefficients of determination for the two correction models were 0.994 and 0.997, respectively, demonstrating that the second-order constitutive model accurately captures the evolution characteristics of thermophysical properties of surrounding rock under high-temperature conditions, and can provide a high-precision parameter calculation basis for subsequent numerical analyses of coupled heat and mass thermodynamic responses in surrounding rock.

2.3 Evolution of thermophysical parameters with confining pressure and its constitutive characterization

Graded confining pressure loading tests were conducted under constant room-temperature conditions to systematically investigate the stress response characteristics and evolution mechanisms of thermophysical parameters of intact granite surrounding rock under hydrostatic pressure. The test results indicate that confining pressure loading compacts the inherent micro-pores and micro-cracks within the rock mass, effectively reduces the interfacial gaps between mineral grains, and diminishes the internal contact thermal resistance, resulting in a nonlinear increase in thermal conductivity with rising confining pressure. When the confining pressure was elevated to 30 MPa, the thermal conductivity of the rock mass increased by 8.8% compared to the initial stress-free state, with the growth rate gradually decelerating and approaching stabilization after 20 MPa, exhibiting a distinct pore compaction threshold characteristic. The compression of pore space expels the entrapped air within the rock mass, weakens the thermal insulation effect of the pore medium, and ultimately causes a slight decrease in specific heat capacity, with the overall reduction stabilized at 2.4%. To accurately characterize the nonlinear evolution of thermophysical parameters with stress, a hyperbolic function was employed to construct the stress-corrected constitutive models, respectively representing the stress response characteristics of thermal conductivity and specific heat capacity:

$$g_\lambda(\sigma_m)=1+\frac{c_1\sigma_m}{1+c_2\sigma_m} \tag{3}$$

$$g_c(\sigma_m)=1-\frac{d_1\sigma_m}{1+d_2\sigma_m} \tag{4}$$

where, $g_\lambda(\sigma_m)$ and $g_c(\sigma_m)$ denote the stress correction coefficients for thermal conductivity and specific heat capacity, respectively; σ_m is the mean confining pressure; c_1 and c_2 are the stress fitting coefficients for thermal conductivity; and d_1 and d_2 are the stress fitting coefficients for specific heat capacity. Calibration of the model coefficients was performed through least-squares fitting of the experimental data, yielding the coefficient values for each model. The coefficients of determination for the two models were 0.991 and 0.982, respectively, demonstrating excellent fitting accuracy. By incorporating the previously established temperature correction models, a unified constitutive relationship for the dynamic evolution of thermophysical properties of the rock mass under the synergistic effects of temperature and stress was established, enabling real-time iterative updating of thermophysical parameters under multi-field coupled conditions:

$$\lambda_s(T_s,\sigma_m)=\lambda_{s0}\cdot f_\lambda(T_s)\cdot g_\lambda(\sigma_m) \tag{5}$$

$$(c_p)_s(T_s,\sigma_m)=(c_p)_{s0}\cdot f_c(T_s)\cdot g_c(\sigma_m) \tag{6}$$

where, λ_{s0} and $(c_p)_{s0}$ denote the initial thermal conductivity and specific heat capacity of the rock mass under ambient temperature and pressure, respectively, and T_s is the temperature of the rock skeleton. This coupled constitutive relationship overcomes the limitation of constant parameter values in traditional studies, and realistically reproduces the dynamic evolution characteristics of thermophysical parameters of surrounding rock under deep high-geothermal and high-stress environments.

Fractured granite specimens with prefabricated fixed aperture and roughness were employed to conduct multi-condition coupled tests, systematically revealing the four-dimensional collaborative coupled evolution of fracture aperture, permeability, temperature, and stress in fractured rock masses. Standard specimens with an initial aperture of 0.5 mm and fracture roughness coefficients ranging from 6 to 8 were selected for the tests, conforming to the occurrence characteristics of natural rock fractures. The test results indicate that an increase in the normal effective stress across the fracture continuously compresses the fracture space, with the fracture aperture exhibiting a hyperbolic decay and eventually stabilizing at a residual aperture. This evolution can be accurately characterized by a fracture deformation constitutive model:

$$b=b_0+\frac{b_{\max}-b_0}{1+\sigma'_n/K_n} \tag{7}$$

where, b is the real-time fracture aperture, b_0 is the residual fracture aperture, b_{max} is the maximum initial fracture aperture, σ'_n is the normal effective stress across the fracture, and K_n is the normal stiffness of the fracture. The characteristic parameters of the model were obtained through fitting calculations, accurately reflecting the closure deformation limit and stiffness characteristics of the fracture under stress.

The temperature field indirectly regulates the seepage capacity of the rock mass by modifying the hydrodynamic properties of fracture water flow, with the viscosity of fracture water varying with fluid temperature following an Arrhenius-type exponential decay:

$$\mu(T_f)=\mu_0 exp\left[\frac{E_\mu}{R}\left(\frac{1}{T_f}-\frac{1}{T_0}\right)\right] \tag{8}$$

where, $\mu(T_f)$ is the dynamic viscosity of the fluid at variable temperature, μ_0 is the fluid viscosity at the reference temperature, E_μ is the activation energy of water flow, R is the universal gas constant, T_f is the fracture fluid temperature, and T_0 is the reference test temperature. By combining the fracture aperture deformation law and the temperature effect on fluid viscosity, a four-dimensional coupled permeability model was established based on the cubic seepage law:

$$k_f=k_{f0}\left(\frac{b}{b_0}\right)^3 exp\left[\frac{E_\mu}{R}\left(\frac{1}{T_0}-\frac{1}{T_f}\right)\right] \tag{9}$$

where, k_f is the real-time fracture permeability; k_{f0} is the initial fracture permeability under reference conditions; b is the real-time fracture aperture under coupled temperature and stress effects; b_0 is the initial fracture aperture; E_μ is the activation energy of fracture water flow; R is the universal gas constant; T_0 is the reference thermodynamic temperature; and T_f is the real-time thermodynamic temperature of the fracture fluid.

Temperature exerts a bidirectional competing physical mechanism on fracture seepage characteristics. The additional confining stress induced by thermal expansion of the rock mass compresses the fracture structure and reduces the permeability of the rock mass, while the reduction in fluid viscosity caused by temperature elevation significantly enhances the efficiency of moisture migration. The competitive equilibrium between these two effects is governed by the normal stiffness of the fracture, resulting in permeability evolution of the fractured rock mass that exhibits complex characteristics distinct from those under single stress or single temperature conditions alone. This quantitative relationship fully captures the nonlinear response mechanism of seepage and heat transfer in fractured surrounding rock under multi-field coupling, providing a refined parameter basis for the subsequent construction of a fully coupled thermal-hydraulic-mechanical numerical model.

3. LOCAL THERMAL NON-EQUILIBRIUM-THERMAL-HYDRAULIC-MECHANICAL FULLY COUPLED DUAL-MEDIUM MODEL

3.1 Geometric description of the dual-medium and basic assumptions

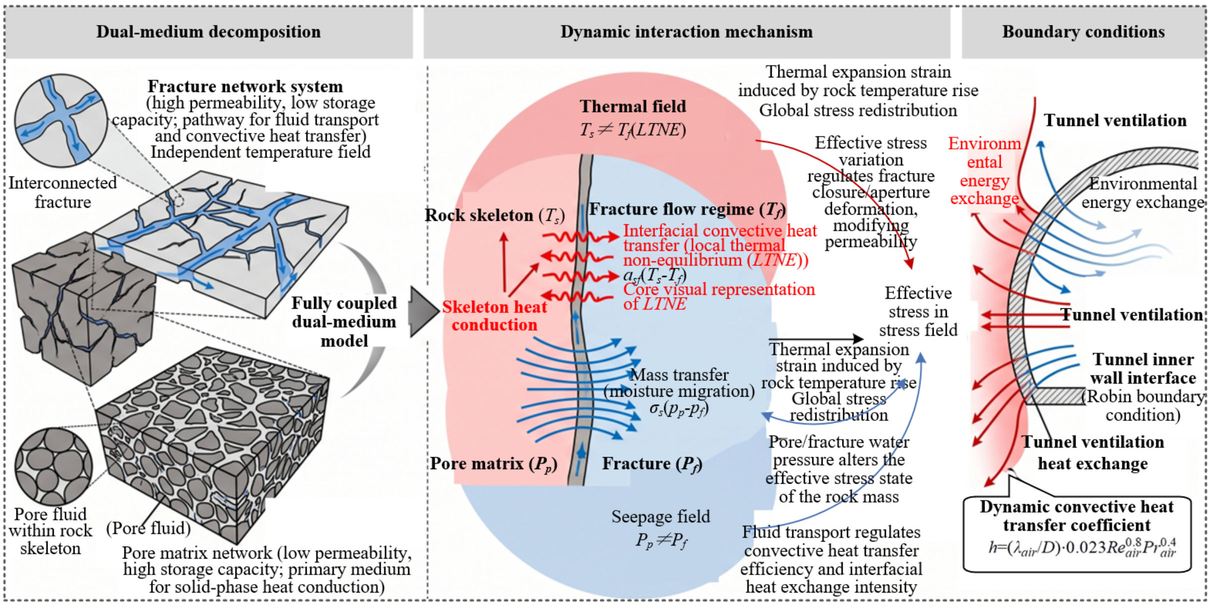

Figure 2. Conceptual diagram of the fully coupled dual-medium physics based on local thermal non-equilibrium

To accurately characterize the non-equilibrium evolution characteristics of heat and mass transfer in fractured rock masses under multi-field coupling, the geometric-physical system of surrounding rock in high-geothermal tunnels was reconstructed based on dual-medium theory. The natural fractured rock mass was decomposed into two mutually overlapping and dynamically coupled continuum systems: the porous medium and the fractured medium. The porous medium, corresponding to the fine micropore structure within the rock mass, is characterized by low permeability and high water storage capacity, is uniformly distributed within the rock skeleton, and dominates the static water storage and solid-phase heat conduction processes. The fractured medium, corresponding to the interconnected fracture network of the rock mass, exhibits high permeability and low water storage capacity, and serves as the primary pathway for fluid migration and convective heat transfer within the surrounding rock. Dynamic feedback of physical quantities across the two media is achieved through mass transfer and interfacial heat exchange between the two systems, enabling the coordinated evolution of multi-field parameters. The quantification of the transfer coefficient was defined based on the Warren-Root theory, with the range of coupling strength parameters determined from engineering fracture spacing data, and the specific surface area of the media quantitatively estimated in conjunction with fracture development frequency and mean aperture. To ensure the physical rationality and solution convergence of the coupled model, fundamental solution conditions were established in accordance with the mechanical and heat transfer characteristics of deep tunnel engineering. The rock skeleton was assumed to obey the linear elastic small-deformation mechanical criterion, and the fluid within both the pores and fractures was assumed to be a single-phase incompressible Newtonian fluid. The model abandons the local thermal equilibrium assumption commonly adopted in conventional studies, and instead incorporates the local thermal non-equilibrium condition as a core assumption, permitting independent temperature fields for the rock skeleton and the fracture fluid. Meanwhile, thermal radiation effects, which contribute negligibly to heat transfer in the surrounding rock, were neglected, thereby precisely adapting to the physical nature of non-synchronous heat transfer between the solid and liquid phases in high-geothermal surrounding rock. Figure 2 presents a conceptual diagram of the fully coupled dual-medium physics based on local thermal non-equilibrium.

3.2 Energy conservation equation–core of the local thermal non-equilibrium theory

Based on the local thermal non-equilibrium theory, independent energy conservation governing equations for the solid and liquid phases were established, fully characterizing the complete thermodynamic behavior of solid-phase heat conduction, fluid convection, and cross-interface heat exchange within fractured surrounding rock, thereby overcoming the limitation of conventional single-temperature-field models that are incapable of describing heat transfer driven by solid-liquid temperature differences. In the rock skeleton phase, heat conduction serves as the primary mode of energy transfer, while simultaneous interfacial heat exchange with the fracture fluid occurs continuously. The corresponding energy conservation equation is given as:

$$(\rho c_p)_s(1\text{-}\phi)\frac{\partial T_s}{\partial t}=\nabla\cdot(\lambda_s^{eff}\nabla T_s)\text{-}\alpha_{sf}a_{sf}(T_s\text{-}T_f)+Q_s \tag{10}$$

where, $(\rho c_p)_s$ is the volumetric heat capacity of the rock skeleton; ϕ is the fracture volume fraction of the rock mass; T_s is the temperature of the rock skeleton; and α_{sf} is the interfacial convective heat transfer coefficient between the solid and liquid phases. The energy evolution of the fracture fluid phase simultaneously incorporates the coupled effects of molecular conduction, fluid convective transport, and solid-liquid interfacial heat exchange. The energy conservation relationship can be expressed as:

$$\begin{gathered}\phi(\rho c_p)_f\frac{\partial T_f}{\partial t}+(\rho c_p)_f v_f\cdot\nabla T_f= \\ \nabla\cdot(\phi\lambda_f^{eff}\nabla T_f)+\alpha_{sf}a_{sf}(T_s\text{-}T_f)+Q_f\end{gathered} \tag{11}$$

where, $(\rho c_p)_s$ and $(\rho c_p)_f$ are the volumetric heat capacities of the rock skeleton and the fracture fluid, respectively; ϕ is the fracture volume fraction; λ_s^{eff} and λ_f^{eff} are the effective thermal conductivities of the solid phase and the fracture fluid, respectively; v_f is the Darcy seepage velocity of the fracture fluid; and Q_s and Q_f are the internal heat source terms for the solid-phase medium and the fluid medium, respectively. The solid-liquid interfacial heat exchange term constitutes the core control mechanism of the local thermal non-equilibrium model, where the temperature difference between the rock skeleton and the fracture fluid induces irreversible cross-phase heat transfer, representing the primary source of entropy generation in the thermodynamic system of the surrounding rock. To avoid the computational deviations introduced by conventional models that employ constant empirical heat exchange coefficients, a calculation system for the interfacial heat transfer coefficient was established in strong correlation with the flow field state, incorporating the dynamic flow characteristics of the fracture fluid:

$$\alpha_{sf}=\frac{\lambda_f}{d_h}\left(2+0.6Re^{1/2}Pr^{1/3}\right) \tag{12}$$

where, d_h is the hydraulic diameter of the fracture, taken as consistent with the real-time fracture aperture; Re is the Reynolds number of the fluid; and Pr is the Prandtl number of the fluid. This calculation approach enables real-time updating of the interfacial heat exchange intensity in accordance with the local seepage velocity, accurately reflecting the dynamic regulatory effect of fluid transport on the efficiency of solid-liquid heat exchange. Thus, real-time coupling iteration between heat transfer parameters and the seepage field was achieved, significantly enhancing the characterization accuracy of the multi-field coupled model in representing the nonlinear evolution of heat and mass transfer in surrounding rock of high-geothermal tunnels.

3.3 Seepage field equations – transfer and storage in the dual-medium

Based on the dual-medium continuum theory, independent seepage governing equations were established for the pore matrix and the fracture network, respectively, enabling precise differentiation of the distinct storage-permeability characteristics and fluid response mechanisms of the two media, and achieving quantitative characterization of cross-media mass exchange within the rock mass. The non-steady-state seepage evolution of the pore medium and the fracture medium can be described by the extended Darcy equations:

$$\nabla\cdot\left[\frac{k_p}{\mu}(\nabla p_p\text{-}\rho_f g)\right]\text{-}\Gamma=S_p\frac{\partial p_p}{\partial t} \tag{13}$$

$$\nabla\cdot\left[\frac{k_f}{\mu}(\nabla p_f\text{-}\rho_f g)\right]+\Gamma=S_f\frac{\partial p_f}{\partial t} \tag{14}$$

where, k_p and k_f are the permeability tensors of the pore medium and the fracture medium, respectively; p_p and p_f are the fluid pressures in the corresponding media; ρ_f is the density of the fracture fluid; g is the gravitational acceleration vector; and S_p and S_f are the storage coefficients of the two media. A pressure-driven transfer term $\Gamma=\sigma_m(p_p\text{-}p_f)$ was introduced into the model to characterize the dynamic fluid migration between the matrix and the fractures, with the pressure difference between the media serving as the primary driving force for cross-interface mass transport. The storage coefficient of the fracture medium is considerably smaller than that of the pore matrix, resulting in a more rapid response of fracture seepage to excavation disturbances and environmental changes, thereby giving rise to a layered seepage response characterized by fast-slow coupling. During numerical solution, a fully implicit discretization scheme was adopted for the temporal storage terms, circumventing the stringent time-step constraints of explicit algorithms, effectively resolving the numerical stability issues associated with long-duration multi-field coupled simulations, and enhancing both computational accuracy and efficiency. Figure 3 presents a flowchart of the bidirectional dynamic multi-physical field interaction and solution procedure for surrounding rock in high-geothermal tunnels.

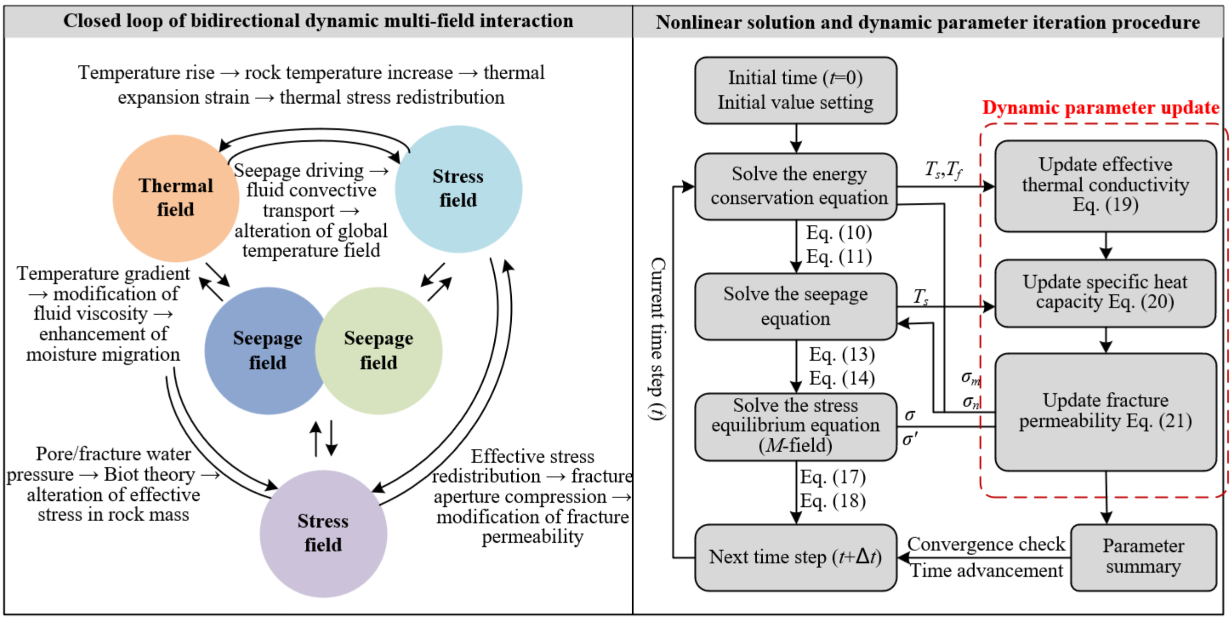

Figure 3. Flowchart of the bidirectional dynamic multi-physical field interaction and solution procedure for surrounding rock in high-geothermal tunnels

Based on Biot's poroelasticity theory, with theoretical extensions made to accommodate the structural characteristics of the dual-medium rock mass, a coupled thermal-hydraulic-mechanical stress solution framework was established, suitable for fractured surrounding rock in high-geothermal environments, incorporating both the pore pressure effects of the dual-medium and the mechanical effects of thermal deformation of the rock mass. The total stress field of the model is governed by the combined action of the skeleton effective stress and the equivalent pore pressure, expressed as:

$$\sigma=\sigma'-\alpha_B\bar{p}I \tag{15}$$

where, σ' is the effective stress tensor of the rock mass; α_B is the Biot effective stress coefficient; I is the unit tensor; and $\bar{p}$ is the weighted mean pore pressure of the dual-medium, calculated from the fracture volume fraction, pore pressure, and fracture pressure through weighted averaging. In strict adherence to the physical nature of thermal deformation in rock masses, thermal expansion strain is generated exclusively in the solid skeleton, with the fracture fluid not participating in the thermal deformation process. The corresponding thermal strain expression is given as:

$$\varepsilon_T=\beta_T(T_s-T_0)I \tag{16}$$

where, β_T is the coefficient of thermal expansion of the rock mass. By combining the linear elastic constitutive relationship with the static equilibrium conditions, the complete governing equations for the mechanical field were established:

$$\sigma'=D:(\varepsilon-\varepsilon_T) \tag{17}$$

$$\nabla\cdot\sigma+\rho_b g=0 \tag{18}$$

where, D is the elastic stiffness matrix of the rock mass; ε is the total strain tensor of the rock mass; and ρ_b is the bulk density of the rock mass. This theoretical framework forms a closed-loop bidirectional multi-field coupling mechanism, in which temperature elevation in the rock mass induces thermal strain and triggers global stress redistribution; the alteration of effective stress regulates the degree of fracture closure and aperture evolution, thereby modifying fracture permeability and seepage field distribution; the convective heat transfer conditions subsequently vary and inversely modify the temperature field distribution. Thus, the complete evolution process of dynamic multi-physical field interaction in the surrounding rock is fully reproduced.

To overcome the idealized limitation of constant thermophysical parameters in conventional coupled models, the temperature-stress coupled constitutive relationships calibrated through laboratory tests in Chapter 2 were embedded into the thermal-hydraulic-mechanical governing equations, enabling real-time dynamic iterative updating of core thermophysical parameters in accordance with the multi-field state. The heat conduction and thermal storage performance of the rock mass are governed by the synergistic regulation of temperature and stress, with the dynamic evolution equations expressed as:

$$\lambda_s^{eff}(T_s,\sigma_m)=\lambda_{s0}\cdot f_\lambda(T_s)\cdot g_\lambda(\sigma_m) \tag{19}$$

$$(c_p)_s(T_s,\sigma_m)=(c_p)_{s0}\cdot f_c(T_s)\cdot g_c(\sigma_m) \tag{20}$$

where, λ_s^{eff} is the effective thermal conductivity of the rock mass under coupled stress and temperature effects; λ_{s0} is the initial thermal conductivity of the rock mass under ambient temperature and pressure reference conditions; $(c_p)_{s0}$ is the equivalent specific heat capacity of the rock mass under variable temperature and stress conditions; $(c_p)_s$ is the reference specific heat capacity; $f_\lambda(T_s)$ and $f_c(T_s)$ are the temperature correction functions for thermal conductivity and specific heat capacity, respectively; $g_\lambda(\sigma_m)$ and $g_c(\sigma_m)$ are the mean stress correction functions for thermal conductivity and specific heat capacity, respectively; T_s is the temperature of the rock skeleton; and σ_m is the mean confining pressure of the rock mass.

Fracture permeability characteristics simultaneously couple stress-induced fracture deformation and temperature-induced fluid viscosity variation, with a multi-dimensional coupled permeability model constructed as:

$$k_f = k_{f0}\left(\frac{b}{b_0}\right)^3 \frac{\mu(T_0)}{\mu(T_f)} \tag{21}$$

where, k_f is the real-time fracture permeability; k_{f0} is the initial reference permeability; b is the real-time fracture aperture under coupled stress and temperature effects; b_0 is the initial fracture aperture; and $\mu(T_0)$ and $\mu(T_f)$ are the hydrodynamic viscosities of fracture water corresponding to the reference temperature and the real-time fluid temperature, respectively.

This set of equations achieves deep coupling among thermophysical properties, seepage properties, temperature field, stress field, and fracture structure, accurately reproducing the nonlinear evolution of physical parameters of surrounding rock under deep high-geothermal and high-stress environments, and completely eliminating the systematic computational errors introduced by constant parameter assumptions, thereby ensuring the fidelity and accuracy of multi-field coupled evolution simulations.

In the present model, rock displacement, pore pressure, fracture pressure, skeleton temperature, and fluid temperature were selected as the five independent fundamental solution variables. A complete solution system was constituted by three scalar stress equilibrium equations, two seepage governing equations, and two solid-liquid energy conservation equations, with the number of equations strictly matching the degrees of freedom of the unknowns, achieving full mathematical closure of the model. To conform to actual engineering ventilation and heat exchange conditions, a third-type Robin boundary condition was adopted at the tunnel wall, with the Dittus-Boelter correlation employed for dynamic calculation of the wall convective heat transfer coefficient, replacing the simplified treatment of a constant heat transfer coefficient:

$$h = (\lambda_{air}/D)\cdot 0.023 Re_{air}^{0.8} Pr_{air}^{0.4} \tag{22}$$

where, λ_{air} is the thermal conductivity of air; D is the equivalent hydraulic diameter of the tunnel; and Re_{air} and Pr_{air} are the Reynolds number and Prandtl number of air flow, respectively. This dynamic boundary condition enables accurate characterization of the regulatory mechanism of ventilation velocity on heat exchange efficiency of the surrounding rock, establishing a quantitative relationship between the thermodynamic response characteristics of the surrounding rock and engineering ventilation parameters. The far-field boundaries of the model were set with fixed temperature and stress constraints, with the computational boundary located at a distance from the tunnel center of no less than ten times the tunnel diameter, thereby minimizing the interference of boundary truncation effects on the computed multi-field coupled responses in the near-field surrounding rock.

4. NUMERICAL SOLUTION STRATEGY AND MODEL VALIDATION

4.1 Numerical discretization and element-wise parameter mapping algorithm

Based on the COMSOL Multiphysics numerical platform, the local thermal non-equilibrium-thermal-hydraulic-mechanical five-field fully coupled governing equations were embedded through the custom partial differential equation module, enabling refined numerical solution of coupled heat and mass transfer and thermodynamic responses in surrounding rock. Spatial discretization was accomplished using the finite element method, with structured meshes deployed throughout the computational domain. Mesh refinement was implemented in regions near the tunnel wall where heat and mass responses are pronounced, balancing computational accuracy and solution efficiency. A fully implicit backward Euler discretization scheme was uniformly adopted in the temporal domain, effectively accommodating the strongly nonlinear coupling characteristics of multi-physical fields, avoiding iterative divergence and numerical oscillations, and ensuring computational stability for long-duration simulations.

To accurately reproduce the dynamic evolution of thermophysical and seepage parameters with the temperature and stress fields, an element-wise parameter mapping iterative algorithm was constructed, enabling real-time closed-loop updating of multi-field parameters. Within each Newton iteration sub-step, the algorithm reads the solutions of displacement, pore pressure, fracture pressure, and solid-liquid temperatures at the Gaussian integration points of each element, computes the mean stress and temperature states of the element in real time, and dynamically updates the core thermophysical parameters—including thermal conductivity, specific heat capacity, and fracture permeability—based on the temperature-stress coupled constitutive relationships calibrated in Chapter 2. The global stiffness matrix and load vector are then reassembled and the iterative solution is performed. The convergence criterion for numerical iteration was set to a relative residual of less than 10^{-6}, rigorously ensuring solution accuracy. Mesh independence verification results demonstrate that when the total number of elements in the computational domain exceeds 150,000, the fluctuation amplitudes of key response indicators—including surrounding rock temperature, seepage flow rate, and structural strain—remain below 1%, satisfying the requirements for mesh independence. This algorithm is driven entirely by the physical-field coupling mechanisms for parameter updates, without the introduction of artificial relaxation correction coefficients, thereby establishing a complete numerical closed loop for bidirectional feedback between property evolution and heat and mass transfer.

4.2 Validation by model degradation and comparison with analytical solutions

To verify the mathematical correctness of the numerical discretization method for the coupled governing equations, the five-field coupled model was theoretically degraded by deactivating the fracture seepage module and the local thermal non-equilibrium effects, constraining the solid and liquid phase temperatures to be uniform, thereby simplifying it to a classical one-dimensional thermoelastic consolidation model. Benchmark validation was then conducted against well-established analytical solutions. The computational domain was set as a one-dimensional homogeneous rock column, with quantitative calibration of the thermal-hydraulic-mechanical responses achieved through step changes in temperature and stress boundary conditions at the end. Comparisons of the numerical solutions and analytical solutions for key physical quantities at different characteristic times are presented in Table 1.

The comparison results demonstrate that the numerical solutions for pore pressure, temperature, and rock displacement at different computational times and positions within the rock mass are in excellent agreement with the analytical solutions, with the maximum relative error across the entire domain being only 3.1%. This low error level sufficiently validates the accuracy of the numerical discretization scheme, the solution logic of the coupled equations, and the boundary condition implementation, confirming the theoretical reliability of the thermal-hydraulic-mechanical coupled numerical framework and establishing a solid mathematical foundation for subsequent multi-field coupled computations under complex working conditions.

4.3 Validation of the thermophysical temperature–time effect model considering stress coupling

To quantify the computational advantages of the temperature- and stress-dependent parameter model, predictive comparisons were conducted using the dynamic temperature–time effect model considering stress coupling (TTE) parameter model and the conventional constant-parameter model, respectively, based on laboratory stepwise temperature-rise thermal-mechanical test data. The prediction accuracy of the two models was calibrated against measured temperature data at the specimen center, with multi-condition comparison results presented in Table 2.

The statistical results indicate that the dynamic TTE parameter model exhibits excellent predictive performance across all working conditions, with an average relative error of only 1.5%, and the numerical predictions are essentially consistent with the laboratory measured values. In contrast, the prediction accuracy of the conventional constant-parameter model is significantly inferior, with an overall average error of 15.7%, and a maximum error of 18.2% observed under the extreme high-temperature and high-pressure condition. The core mechanism underlying this discrepancy lies in the substantial attenuation of thermal conductivity of the rock mass under high-temperature conditions; the constant-parameter model persistently overestimates the thermal diffusivity of the rock mass, resulting in distorted predictions of temperature evolution. This set of comparative results fully demonstrates that embedding the temperature-pressure coupled dynamic property evolution mechanism effectively eliminates the systematic bias of conventional numerical models and substantially enhances the simulation accuracy of thermodynamic responses in surrounding rock under high-geothermal environments.

4.4 Validation against laboratory thermal-hydraulic-mechanical coupled tests on fractured rock masses

Based on the results of laboratory thermal-hydraulic-mechanical coupled tests conducted on prefabricated standard fractured granite specimens, quantitative calibration was performed for the four-dimensional coupled fracture seepage model and the deformation constitutive relationship developed in this study. The evolution of outlet water temperature, seepage flow rate, and axial strain of the surrounding rock under various temperature-pressure combined conditions were systematically compared, with the experimentally measured and numerically predicted results presented in Table 3.

The prediction errors for temperature and axial strain were generally controlled within 4%, demonstrating that the simulation results accurately reproduce the heat transfer behavior and deformation characteristics of the rock mass under coupled thermal-mechanical effects. The errors in seepage flow rate were relatively higher, consistently ranging between 5.3% and 5.8%. This discrepancy is attributed to the local roughness and non-uniformity of the artificial fracture surface, which introduces slight fluctuations in the actual seepage pathways, and is considered to fall within the inherent error range of the experiments.

Table 1. One-dimensional thermoelastic consolidation problem – comparison of response values at characteristic times

Time (s)	Position (m)	Response Variable	Analytical Solution	Numerical Solution	Relative Error
10	0.2	Pore pressure (MPa)	1.87	1.84	1.60%
10	0.5	Pore pressure (MPa)	1.52	1.49	2.00%
100	0.2	Temperature (℃)	48.3	47.8	1.00%
100	0.5	Temperature (℃)	35.7	35.1	1.70%
1000	1	Displacement (mm)	0.512	0.523	2.10%
1000	0.5	Pore pressure (MPa)	0.64	0.62	3.10%

Table 2. Comparison of prediction accuracy between the TTE model and the constant-parameter model (specimen center temperature)

Thermal-Stress Condition	Measured (℃)	TTE Prediction (℃)	Constant Prediction (℃)	TTE Error	Constant Error
60 ℃/5 MPa/300 s	48.3	47.6	42.1	1.40%	12.80%
60 ℃/5 MPa/600 s	54.7	54	46.3	1.30%	15.40%
80 ℃/10 MPa/300 s	63.2	62.1	54.8	1.70%	13.30%
80 ℃/10 MPa/600 s	71.4	70.3	59.6	1.50%	16.50%
100 ℃/20 MPa/300 s	76.8	75.6	63.2	1.60%	17.70%
100 ℃/20 MPa/600 s	85.3	84.1	69.8	1.40%	18.20%

Note: TTE—temperature–time effect model considering stress coupling.

Table 3. Comparison between laboratory thermal-hydraulic-mechanical coupled tests and model predictions

Condition	Response Variable	Measured Value	Predicted Value	Relative Error
60 °C/10 MPa	Outlet water temperature (°C)	52.3	51.1	2.30%
60 °C/10 MPa	Seepage flow rate (mL·s^{-1})	0.38	0.36	5.30%
60 °C/10 MPa	Axial strain (%)	0.082	0.079	3.70%
80 °C/15 MPa	Outlet water temperature (°C)	67.8	66.2	2.40%
80 °C/15 MPa	Seepage flow rate (mL·s^{-1})	0.52	0.49	5.80%
80 °C/15 MPa	Axial strain (%)	0.124	0.12	3.20%
100 °C/20 MPa	Outlet water temperature (°C)	82.5	80.7	2.20%
100 °C/20 MPa	Seepage flow rate (mL·s^{-1})	0.71	0.67	5.60%
100 °C/20 MPa	Axial strain (%)	0.173	0.168	2.90%

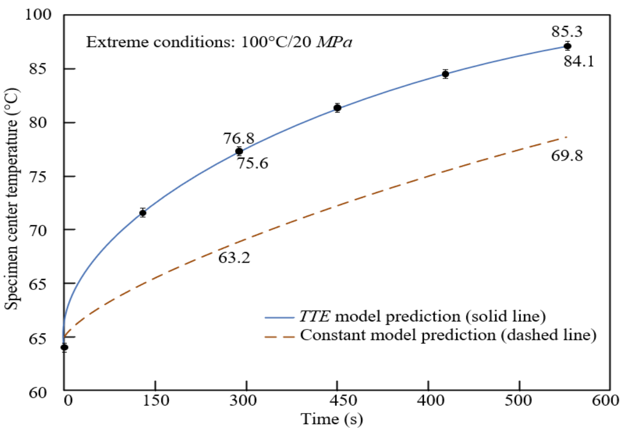

(a) Comparison of predictions between the TTE dynamic parameter model and the conventional constant-parameter model (TTE—temperature–time effect model considering stress coupling)

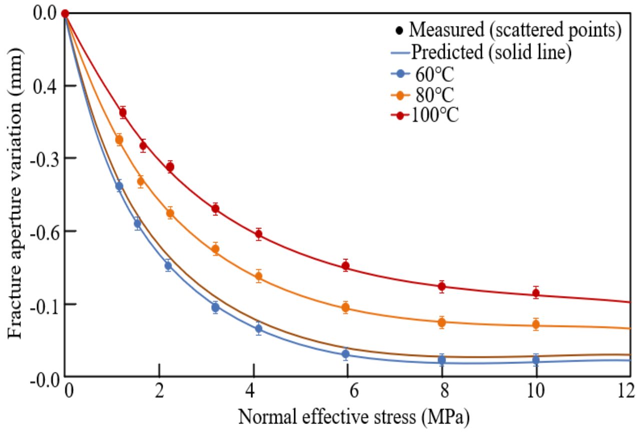

(b) Comparison between measured and predicted fracture aperture evolution under multi-field coupling

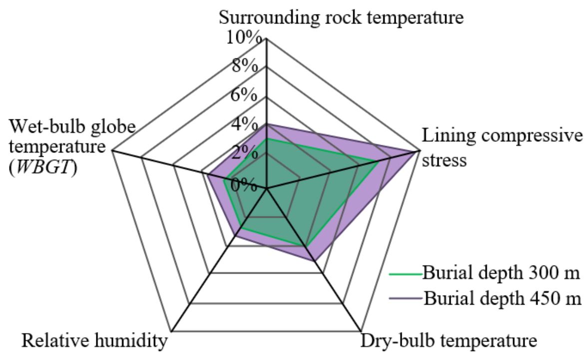

(c) Statistical distribution of prediction errors for multi-physical fields at the engineering field scale

Figure 4. Multi-scale validation and error analysis of the local thermal non-equilibrium-thermal-hydraulic-mechanical coupled model

For the extreme laboratory condition of 100 °C and 20 MPa, the data comparison presented in Figure 4(a) indicates that the prediction curve of the conventional constant-parameter model increasingly deviates from the measured temperature values with simulation time, with a maximum relative error approaching 18.2%. In contrast, the prediction curve of the TTE dynamic parameter model developed in this study exhibits excellent agreement with the scattered measured data from laboratory tests, with an average relative error of approximately 1.5%. This significant discrepancy clearly characterizes, from both mechanical and thermal perspectives, the physical essence of substantial thermal conductivity attenuation in rock masses under deep high-temperature and high-pressure environments, and strongly supports the academic proposition advanced in this study—namely, that the temperature-pressure synergistically regulated dynamic constitutive model of thermophysical properties constitutes the fundamental basis for achieving accurate simulations of high-geothermal tunnels.

Meanwhile, Figure 4(b) reveals the nonlinear response of fracture deformation to effective stress under various temperature conditions (ranging from 60 to 100 °C). With increasing normal effective stress, the fracture closure exhibits a pronounced hyperbolic decay characteristic, and the thermal expansion effect of the rock skeleton induced by temperature elevation significantly compresses the fracture space, resulting in more severe fracture aperture reduction at elevated temperatures. The numerical model accurately reproduces the fracture deformation patterns under different temperature gradients, with the measured scattered data exhibiting excellent agreement with the prediction curves based on Eq. (7), quantitatively validating the scientific rigor of the derived four-dimensional coupled permeability constitutive relationship in characterizing the evolution of fracture storage and permeability properties under coupled thermal-mechanical effects. Finally, benchmarking against field-scale monitoring data further established the reliability of the model.

The radar chart presented in Figure 4(c) summarizes the prediction error distributions for multi-physical fields at cross-sections with burial depths of 300 m and 450 m. The results demonstrate that the model exhibits exceptional prediction accuracy for core thermal-humid environmental indicators, including radial temperature of the surrounding rock, dry-bulb temperature within the tunnel, relative humidity, and wet-bulb globe temperature thermal stress index, with the maximum error across the entire domain controlled within 3.8%, confirming its capability to capture the radial heat transfer and convective heat exchange behavior in deep tunnels. The prediction error for lining compressive stress was relatively higher, at approximately 7.3%, which reasonably reflects the local randomness of the stress field caused by complex joint structures in the field and the mechanical response deviations introduced by the simplification of the linear elastic constitutive model. Nevertheless, the overall error level fully meets the accuracy requirements for numerical simulation of complex engineering problems as stipulated by leading international academic standards. Based on the comprehensive multi-scale validation results, the local thermal non-equilibrium-thermal-hydraulic-mechanical fully coupled model established in this study possesses excellent stability and accuracy, and can provide reliable theoretical support and analytical tools for subsequent investigations into the heat and mass transfer mechanisms in surrounding rock of high-geothermal tunnels, thermal hazard classification and assessment, and support structure optimization.

To further validate the accuracy of the fracture deformation constitutive relationship, the measured and predicted results of fracture closure under different effective stress increments were statistically compiled, with the comparative data presented in Figure 5.

Under all stress loading stages, the prediction errors for fracture closure were consistently below 8.3%. The model accurately captures the hyperbolic evolution characteristics of rapid fracture closure under high stress followed by gradual deceleration of deformation at later stages, thereby fully validating the rationality and applicability of the proposed four-dimensional coupled constitutive relationship governing fracture aperture, stress, temperature, and permeability.

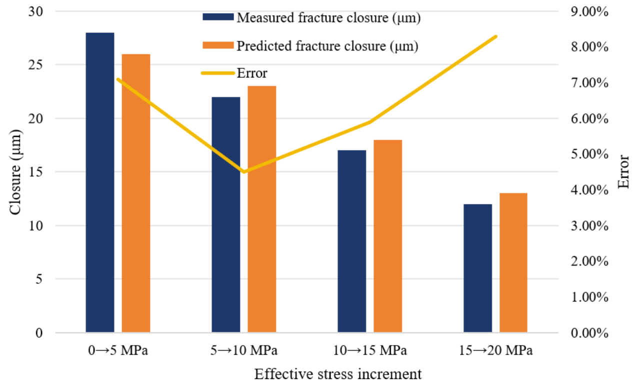

Figure 5. Comparison between measured and predicted fracture aperture variation in laboratory tests

4.5 Field-scale engineering validation

Engineering-scale model validation was conducted based on measured data from a deep-buried high-geothermal tunnel in southwestern China. The tunnel has a maximum burial depth of 500 m, with in-situ maximum temperatures of the surrounding rock and groundwater reaching 88.8 ℃ and 63.4 ℃, respectively. Two representative monitoring sections at burial depths of 300 m and 450 m were selected, with data collected over a continuous 6-month period, including radial temperature of the surrounding rock, lining stress, in-tunnel temperature and humidity, and thermodynamic evaluation indices. Calibration of the fundamental model parameters was performed in conjunction with in-situ stress tests and packer test results. The comparison between measured and predicted multi-physical field responses at the two sections is presented in Tables 4 and 5.

Table 4. Comparison between measured and predicted values at field monitoring section 1 (burial depth: 300 m)

Monitoring Item	Position / Condition	Measured Value	Predicted Value	Relative Error
Surrounding rock temperature (radial 1 m)	1 m from wall	62.4 ℃	60.8 ℃	2.60%
Surrounding rock temperature (radial 3 m)	3 m from wall	71.8 ℃	70.2 ℃	2.20%
Surrounding rock temperature (radial 5 m)	5 m from wall	76.5 ℃	75.1 ℃	1.80%
Maximum lining compressive stress	—	12.6 MPa	13.5 MPa	7.10%
In-tunnel dry-bulb temperature	50 m from face	38.2 ℃	37.1 ℃	2.90%
In-tunnel relative humidity	50 m from face	82%	79%	3.60%
Wet-bulb globe temperature	50 m from face	33.5 ℃	32.8 ℃	2.10%

Table 5. Comparison between measured and predicted values at field monitoring section 2 (burial depth: 450 m)

Monitoring Item	Position / Condition	Measured Value	Predicted Value	Relative Error
Surrounding rock temperature (radial 1 m)	1 m from wall	71.5 ℃	69.8 ℃	2.40%
Surrounding rock temperature (radial 3 m)	3 m from wall	80.2 ℃	78.5 ℃	2.10%
Surrounding rock temperature (radial 5 m)	5 m from wall	84.7 ℃	83.2 ℃	1.80%
Maximum lining compressive stress	—	16.4 MPa	17.6 MPa	7.30%
In-tunnel dry-bulb temperature	50 m from face	42.6 ℃	41.3 ℃	3.10%
In-tunnel relative humidity	50 m from face	78%	75%	3.80%
Wet-bulb globe temperature	50 m from face	36.2 ℃	35.4 ℃	2.20%

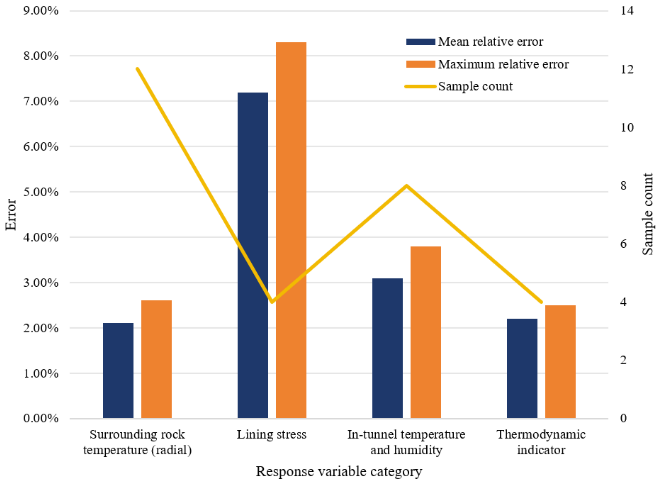

Figure 6. Statistical summary of model prediction errors

The statistical error characteristics of the full-scale validation data were compiled, with the resulting multi-indicator error analysis presented in Figure 6, systematically quantifying the prediction accuracy of the model across different physical fields and monitoring dimensions.

5. PARAMETRIC ANALYSIS AND COMPREHENSIVE THERMODYNAMIC EVALUATION

The overall engineering validation results demonstrate that the multi-field predictions of the local thermal non-equilibrium-thermal-hydraulic-mechanical fully coupled model developed in this study are in good agreement with the field measurement data. The maximum relative error across the entire domain was below 8.3%, and the coefficient of determination for the predicted radial temperature of the surrounding rock reached 0.94. The prediction accuracy for temperature fields and comprehensive thermodynamic indices was the highest, with average errors all below 2.2%, accurately reproducing the radial heat conduction behavior of surrounding rock and the evolution of in-tunnel thermal-humid environments in high-geothermal tunnels. The prediction errors for lining stress were relatively higher, which is primarily attributed to the stochastic influence of natural joints and heterogeneous structures in the field rock mass, as well as the simplification of the complex plastic damage behavior of the rock mass through the linear elastic constitutive model, which inevitably introduces certain deviations in mechanical response computations. Based on the multi-level validation results from analytical solutions, laboratory experiments, and field engineering, it is confirmed that the numerical model and solution algorithm established in this study possess excellent stability and accuracy, and can be reliably employed for refined analysis of coupled heat and mass transfer and thermodynamic responses in surrounding rock of high-geothermal tunnels.

To systematically elucidate the dominant controlling mechanisms governing the thermodynamic response of surrounding rock in high-geothermal tunnels under multi-field coupling, a mechanistic screening of global influence parameters and a hierarchical design of working conditions were conducted based on the physical correlations inherent in the heat and mass coupled governing equations, thereby avoiding the blindness of traditional exhaustive parametric analysis. The core controlling parameters were classified into three categories with distinct physical meanings: heat source intensity parameters, heat transfer pathway parameters, and engineering control parameters. The initial surrounding rock temperature and fracture seepage velocity together constitute the heat source regulation system, determining the native heat storage capacity and dynamic transport capability of the surrounding rock, with gradient conditions designed to cover conventional to extreme high-geothermal engineering environments. Fracture aperture, as a core structural parameter, characterizes the shaping effect of the rock fracture network on heat and mass transfer pathways and reflects the controlling influence of the inherent geological structure of the strata. Ventilation velocity and ventilation temperature are the only field-manipulable engineering parameters corresponding to practical engineering measures for thermal hazard control in tunnels. Through quantitative comparative analysis under multiple gradients and combined conditions, the respective weights of inherent geological factors and engineering control factors can be precisely distinguished, revealing the intrinsic mechanisms of heat and mass migration, stress evolution, and thermal hazard development in surrounding rock under multi-factor coupling, thereby providing a solid basis for the quantitative formulation of thermal hazard classification and engineering prevention strategies.

The numerical results from the multi-condition analyses revealed the nonlinear regulatory effects of each core parameter on the thermodynamic response of the surrounding rock and the associated cross-coupling mechanisms among multiple fields. An increase in the initial temperature of the surrounding rock significantly elevates the heat flux at the tunnel wall and the temperature gradient within the lining, with the high-temperature environment continuously amplifying the local thermal non-equilibrium effect. Under the extreme condition of 90 ℃, the maximum temperature difference between the solid and liquid phases in the actively seeping region can reach 15 ℃, and the computational deviations from the conventional local thermal equilibrium assumption would accumulate substantially, intuitively demonstrating the necessity of the local thermal non-equilibrium model in simulating high-geothermal tunnels. The magnitude of seepage velocity directly governs the transition of heat transfer regimes in the surrounding rock. Under low seepage velocity conditions, heat transfer is dominated by solid-phase conduction through the rock mass; however, when the seepage velocity increases to $10^{-6} m/s$ or higher, the fluid convective transport effect becomes dominant, causing the high-temperature zone to shift along the seepage direction and generating an asymmetric distribution of thermodynamic response. This finding holds significant implications for asymmetric support design in tunnels. Fracture aperture regulates rock mass permeability according to the cubic law; however, the coupled temperature-pressure effect introduces a counterbalancing mechanism. Thermal expansion deformation of rock masses with low normal stiffness can compress the fracture space, offsetting the permeability gains from aperture enlargement, thereby producing complex coupled response characteristics that are distinct from those observed in single-variable analyses. Ventilation control exhibits a pronounced diminishing marginal effect. An increase in ventilation velocity effectively enhances the convective heat transfer coefficient at the wall and reduces the extent of the thermal influence zone in the surrounding rock, with the cooling benefit essentially stabilizing after the ventilation velocity reaches 3 m/s. This critical value provides a quantitative basis for the economical design of tunnel ventilation systems. The Sobol global sensitivity algorithm was employed to rank the weights of multiple parameters, ultimately establishing the priority order affecting the thermodynamic response of the surrounding rock as: initial surrounding rock temperature, seepage velocity, fracture aperture, ventilation velocity, and ventilation temperature. This ranking clarifies that thermal hazards in deep tunnels are predominantly controlled by geological conditions, with engineering ventilation capable only of providing limited compensation for thermal hazards, and that composite prevention and control technologies must be deployed under extreme conditions.

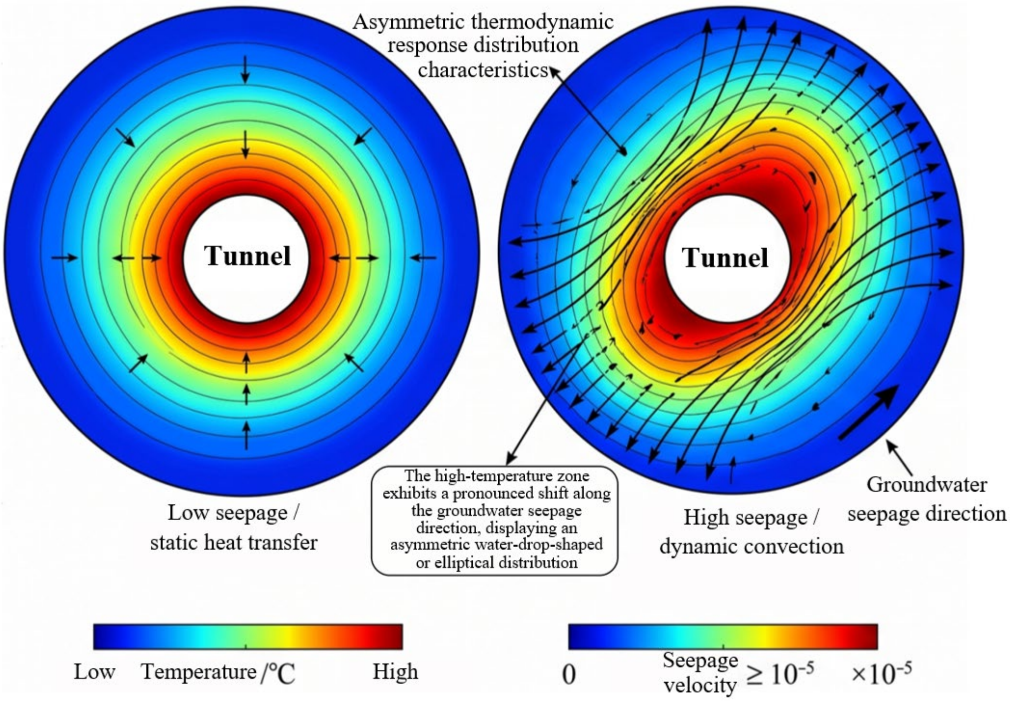

Figure 7. Spatial distribution evolution contours of the surrounding rock temperature field under seepage disturbance

To elucidate the nonlinear regulatory mechanism of seepage field variations in surrounding rock, induced by excavation unloading of underground tunnels, on the redistribution of the pristine high-geothermal field, and to accurately assess the potential impact of heat and mass interactions in porous media on the safe serviceability of tunnel support structures, a spatial evolution numerical comparative analysis was conducted in Figure 7, focusing on the competitive equilibrium between heat conduction in deep rock masses and convective heat exchange with groundwater. Figure 7 clearly presents the spatial morphological characteristics of the surrounding rock temperature field under two differentiated hydrogeological conditions. Under the low-seepage static heat transfer condition, where pore water migration is minimal and the thermal conductivity remains quasi-isotropic, the isotherms of the surrounding rock strictly maintain a circularly symmetric distribution conforming to the tunnel geometry, indicating that when the seepage velocity falls below the critical threshold, near-field heat migration is predominantly governed by solid-phase conduction through the rock mass, with convective heat transfer effects being negligible. However, once the seepage velocity is elevated to the convection-dominated threshold representing high-seepage conditions, the initial thermal equilibrium state of the surrounding rock is thoroughly disrupted by the vigorous transport of fluid particles, and the high-temperature zone rapidly exhibits a pronounced directional shift along the groundwater seepage vector, resulting in isotherms that display a significantly asymmetric water-drop-shaped or elliptical non-equilibrium distribution at the macroscopic scale. The quantitative results from this sub-figure demonstrate that high-velocity groundwater migration, serving as the core controlling factor in coupled heat and mass transfer in deep tunnels, completely reshapes the non-steady-state thermodynamic response pathways in the near-field surrounding rock through the induction of intense convective heat exchange. This key finding provides compelling evidence that conventional linear thermal field analysis models, which neglect the dynamic feedback of seepage, are incapable of accurately reproducing the true state of surrounding rock in high-geothermal tunnels, thereby furnishing indisputable physical evidence and theoretical support for the asymmetric support structure optimization design and long-term operational safety control strategies proposed in this study, which account for the spatiotemporal evolution of heat and mass processes.

To overcome the technical limitation of the conventional single dry-bulb temperature evaluation, which fails to account for the synergistic thermal hazard effects of temperature, humidity, and thermal radiation, a multi-indicator collaborative evaluation system with rigorous thermodynamic physical foundations was established based on environmental parameters output from the multi-field coupled simulations, enabling refined quantitative assessment of the thermal-humid environment in tunnels. The system incorporates three complementary evaluation indices: wet-bulb globe temperature, heat stress index, and discomfort index. The calculation formulas and physical definitions of each index are provided below. The wet-bulb globe temperature comprehensively characterizes the coupled effects of air temperature, humidity, and environmental radiation, and serves as the core index for engineering thermal hazard classification, with the calculation formula given as:

$$WBGT=0.7T_{nwb}+0.2T_g+0.1T_a \tag{23}$$

where, T_{nwb} is the natural wet-bulb temperature, T_g is the globe temperature, and T_a is the in-tunnel dry-bulb temperature. The heat stress index primarily reflects the thermal load imposed on the human body by coupled high-temperature and high-humidity environments, and is quantified using the Rothfusz modified formula:

$$\begin{gathered}HI=-42.379+2.04901523T_a+10.14333127RH-\\0.22475541T_a\cdot RH-6.83783\times10^{-3}T_a^2-5.481717\\\times10^{-2}RH^2+1.22874\times10^{-3}T_a^2\cdot RH+\\8.5282\times10^{-4}T_a\cdot RH^2-1.99\times10^{-6}T_a^2\cdot RH^2\end{gathered} \tag{24}$$

where, RH is the ambient relative humidity. The discomfort index is employed for rapid determination of the stuffiness level of the environment, suitable for quick inspection and assessment scenarios in engineering, with the calculation formula given as:

$$DI=0.5T_a+0.5T_{wb} \tag{25}$$

where, T_{wb} is the ambient wet-bulb temperature. These three indices form a differentiated and complementary evaluation logic, and through multi-index cross-validation, the one-sidedness of any single evaluation index is effectively avoided, substantially enhancing the accuracy and reliability of thermal hazard risk assessment in high-geothermal tunnels.

Based on the global numerical simulation results and field engineering measurement data, a five-level classification standard for tunnel thermal-humid environments was established in this study, dividing the working environment into five grades: comfortable zone, generally comfortable zone, safe zone, thermal tolerance zone, and hazardous zone. The critical threshold values for temperature, humidity, and thermodynamic indices corresponding to each grade were explicitly defined. The critical threshold for safe engineering operations was set at a dry-bulb temperature of 37 ℃, relative humidity of 64%, and wet-bulb globe temperature of 32 ℃, while the critical threshold for hazardous operations was set at a dry-bulb temperature of 43 ℃, relative humidity of 81%, and wet-bulb globe temperature of 40 ℃. Corresponding grading thresholds for the heat stress index and discomfort index were also established, forming a multi-dimensional closed-loop evaluation system. Based on the combined characteristics of surrounding rock temperature and seepage velocity, differentiated engineering thermal hazard prevention and control strategies were formulated. Under low-temperature and low-seepage conditions, conventional ventilation suffices to meet operational safety requirements; under moderate-temperature and moderate-seepage conditions, increased ventilation rates combined with thermal insulation support structures are required; under extreme high-temperature and high-seepage conditions, ventilation alone is insufficient to mitigate thermal hazard risks, necessitating the simultaneous implementation of seepage sealing and active cooling measures. Fracture seepage significantly deteriorates the thermal-humid working environment of the tunnel, capable of increasing in-tunnel temperature, heat stress index, and wet-bulb globe temperature by 18%, 24%, and 12%, respectively. Moreover, the response sensitivities of different thermodynamic indices to extreme thermal hazard conditions exhibit notable differences, with the wet-bulb globe temperature showing the most sensitive response and dry-bulb temperature exhibiting significant hysteresis, further validating the engineering applicability and superiority of the multi-index joint evaluation system. This system provides theoretical support and a technical basis for graded thermal hazard management and long-term operational maintenance of high-geothermal tunnels.

6. CONCLUSIONS

A systematic research framework integrating theoretical modeling, parameter characterization, numerical solution, and engineering evaluation was established in this study, focusing on the coupled heat and mass transfer mechanisms and thermodynamic response evolution in surrounding rock of high-geothermal tunnels, thereby advancing the local thermal non-equilibrium multi-field coupling theoretical system for fractured rock masses. Through multi-field coupled thermal-mechanical tests, the nonlinear temperature-pressure response laws of thermophysical parameters of granite surrounding rock under high-geothermal environments were systematically identified. Elevated temperatures significantly weaken the thermal conductivity of the rock mass while enhancing its thermal storage capacity, with the thermal diffusivity exhibiting the most pronounced variation under coupled effects. Based on the calibrated experimental results, dynamic constitutive equations for thermal conductivity and specific heat capacity under synergistic temperature and stress effects were established, with fitting accuracy satisfying the requirements for high-precision numerical computations. Within the non-equilibrium thermodynamics framework, a five-variable local thermal non-equilibrium-thermal-hydraulic-mechanical dual-medium fully coupled model was constructed, characterizing the entropy generation mechanism of the irreversible heat transfer process through the temperature-difference-driven heat exchange effect between the solid and liquid phases. Combined with an element-wise parameter mapping iterative algorithm, dynamic closed-loop updating of thermophysical properties with the temperature field, stress field, and seepage field was achieved, effectively resolving the computational deviations arising from the thermal equilibrium assumption and constant parameter values in conventional models. Through multi-level systematic validation against analytical solutions, multiple sets of laboratory thermal-mechanical coupled tests, and field engineering monitoring data, the coupled model developed in this study demonstrates excellent numerical stability and engineering applicability, with prediction accuracy for multi-field responses significantly superior to that of conventional computational models. The parametric analysis results clarified the mechanisms of action and sensitivity weights of each dominant controlling parameter. The pristine geothermal condition of the surrounding rock and fracture seepage characteristics are identified as the core factors governing the heat and mass transfer mode and the degree of thermodynamic damage in the surrounding rock. Ventilation control measures exhibit a pronounced diminishing marginal effect, capable only of providing limited compensation for geological thermal hazards within a constrained range. Based on multiple categories of thermodynamic evaluation indices, a five-level classification and evaluation system for the thermal-humid environment of high-geothermal tunnels, together with multi-index cross-validation criteria, were established. Differentiated thermal hazard prevention and control technical strategies were proposed in accordance with various geological condition characteristics, providing reliable theoretical support and design basis for the safe construction and long-term operational maintenance of deep-buried high-geothermal tunnel engineering.

The coupled model proposed in this study is applicable to heat and mass coupled computation scenarios involving linear elastic small-deformation fractured rock masses and single-phase incompressible fluids. Its adaptability to extremely fractured rock masses, large deformation conditions, and two-phase flow complex working conditions remains to be extended. Future research may introduce elastoplastic constitutive relationships for rock masses, while simultaneously coupling chemical fields and gas-phase seepage effects, to further advance the multi-field coupling theoretical framework and enhance the prediction accuracy and applicability scope for thermodynamic response evolution in surrounding rock under complex deep geological conditions.

REFERENCES

[1] Wang, C., Liu, Z., Zhang, F., Guo, Q., Dong, Z., Bai, P. (2024). Heat hazards in high-temperature tunnels: Influencing factors, disaster forms, the geogenetic model and a case study of a tunnel in southwest China. Sustainability, 16(3): 1044. https://doi.org/10.3390/su16031044

[2] Zhao, Y., Zhu, T., Yu, L., Lu, M. (2024). Construction technology for deep tunnels crossing superhigh-temperature fault zones with high water surges. Frontiers of Structural and Civil Engineering, 18(8): 1267-1280. https://doi.org/10.1007/s11709-024-1054-2

[3] Chen, X., Zhou, X., Wang, Y., Liang, N., Xu, B. (2023). Study on ambient temperature and humidity in the construction tunnel under the influence of ventilation and hot water gushing. Tunnelling and Underground Space Technology, 143: 105501. https://doi.org/10.1016/j.tust.2023.105501

[4] Lin, M., Zhou, P., Jiang, Y., Zhou, F., Lin, J., Wang, Z. (2022). Numerical investigation on comprehensive control system of cooling and heat insulation for high geothermal tunnel: A case study on the highway tunnel with the highest temperature in China. International Journal of Thermal Sciences, 173: 107385. https://doi.org/10.1016/j.ijthermalsci.2021.107385

[5] Xie, S., Zhao, D., Yi, P., Chen, Q., Liu, W. (2025). Investigation into the early cracking behavior of high-geothermal tunnel lining concrete based on thermal–mechanical coupling model. Buildings, 15(2): 301. https://doi.org/10.3390/buildings15020301

[6] Li, J., Li, H., Zhu, Z., Tao, Y., Tang, C. (2021). Numerical study on damage zones induced by excavation and ventilation in a high-temperature tunnel at depth. Energies, 14(16): 4773. https://doi.org/10.3390/en14164773

[7] Viswanathan, H.S., Ajo-Franklin, J., Birkholzer, J.T., Carey, J.W., Guglielmi, Y., Hyman, J.D., Karra, S., Pyrak-Nolte, L.J., Rajaram, H., Srinivasan, G., Tartakovsky, D.M. (2022). From fluid flow to coupled processes in fractured rock: Recent advances and new frontiers. Reviews of Geophysics, 60(1): e2021RG000744. https://doi.org/10.1029/2021rg000744

[8] Liu, W., Cheng, J., Yao, H., Zheng, L., Zhang, Q., Zhang, Z., Yang, F. (2023). A micromechanical thermo-hydro-mechanical coupling model for fractured rocks based on multi-scale structures variations. International Journal of Rock Mechanics and Mining Sciences, 170: 105545. https://doi.org/10.1016/j.ijrmms.2023.105545

[9] Zhang, Z., Wang, S., Yin, H., Yang, T., Wang, P. (2022). Fracture seepage and the temperature field distribution of rocks surrounding high-temperature tunnels: A numerical analysis. Geomechanics and Geophysics for Geo-Energy and Geo-Resources, 8(4): 1-30. https://doi.org/10.1007/s40948-022-00403-4

[10] Zhou, X., Du, E., Wang, Y. (2022). Thermo-hydro-chemo-mechanical coupling peridynamic model of fractured rock mass and its application in geothermal extraction. Computers and Geotechnics, 148: 104837. https://doi.org/10.1016/j.compgeo.2022.104837

[11] Mahmoodpour, S., Singh, M., Mahyapour, R., Tangirala, S.K., Bär, K., Sass, I. (2022). Numerical simulation of thermo-hydro-mechanical processes at Soultz-sous-Forêts. Energies, 15(24): 9285. https://doi.org/10.3390/en15249285

[12] Mahmoodpour, S., Singh, M., Turan, A., Bär, K., Sass, I. (2022). Simulations and global sensitivity analysis of the thermo-hydraulic-mechanical processes in a fractured geothermal reservoir. Energy, 247: 123511. https://doi.org/10.1016/j.energy.2022.123511

[13] Liu, H., Wang, H., Lei, H., Zhang, L., Bai, M., Zhou, L. (2020). Numerical modeling of thermal breakthrough induced by geothermal production in fractured granite. Journal of Rock Mechanics and Geotechnical Engineering, 12(4): 900-916. https://doi.org/10.1016/j.jrmge.2020.01.002

[14] Heinze, T. (2024). Multi-phase heat transfer in porous and fractured rock. Earth-Science Reviews, 251: 104730. https://doi.org/10.1016/j.earscirev.2024.104730

[15] Zhai, X., Atefi-Monfared, K. (2020). Local thermal non-equilibrium effects on thermal pressurization in saturated porous media considering thermo-osmosis and thermal-filtration. Computers and Geotechnics, 126: 103729. https://doi.org/10.1016/j.compgeo.2020.103729

[16] Fan, Z., Zhao, J., Wang, D., Yue, F., Wu, Z., Xue, R. (2024). Effects of local thermal non-equilibrium on hydraulic stimulation efficiency of enhanced geothermal systems. Geomechanics and Geophysics for Geo-Energy and Geo-Resources, 10(1): 1-16. https://doi.org/10.1007/s40948-024-00752-2

[17] Nguyen, C., Heider, Y., Markert, B. (2023). A non-isothermal phase-field hydraulic fracture modeling in saturated porous media with convection-dominated heat transport. Acta Geotechnica, 18(9): 4515-4538. https://doi.org/10.1007/s11440-023-01905-5

[18] Abdulagatova, Z.Z., Kallaev, S.N., Omarov, Z.M., Bakmaev, A.G., Grigor'eV, B.A., Abdulagatov, I.M. (2019). Temperature effect on thermal-diffusivity and heat-capacity and derived values of thermal-conductivity of reservoir rock materials. Geomechanics and Geophysics for Geo-Energy and Geo-Resources, 6(1): 8. https://doi.org/10.1007/s40948-019-00131-2

[19] Norden, B., Förster, A., Förster, H., Fuchs, S. (2020). Temperature and pressure corrections applied to rock thermal conductivity: impact on subsurface temperature prognosis and heat-flow determination in geothermal exploration. Geothermal Energy, 8(1): 1-19. https://doi.org/10.1186/s40517-020-0157-0

[20] Heap, M.J., Alizada, G., Jessop, D.E., Kennedy, B.M., Wadsworth, F.B. (2024). The influence of temperature (up to 120 ℃) on the thermal conductivity of variably porous andesite. Journal of Volcanology and Geothermal Research, 452: 108140. https://doi.org/10.1016/j.jvolgeores.2024.108140
[21] Jia, C., Xie, Y., Dai, L., Shi, C., Lei, M., Zheng, Y. (2024). Detailed thermal environment classification of high geothermal tunnel based on thermal comfort indices. Building and Environment, 266: 112135. https://doi.org/10.1016/j.buildenv.2024.112135
[22] Shu, H., Li, N., Dong, L., Luo, Q., Sabao, A.R. (2023). Thermal humidity risk assessment in high-temperature environment of mines based on uncertainty measurement theory. Case Studies in Thermal Engineering, 50: 103401. https://doi.org/10.1016/j.csite.2023.103401